A Two-Dimensional Non-Separable Implementation of Dyadic-Valued Cosine-Sine Modulated Filter Banks for Low Computational Complexity

Seisuke Kyochi*, Taizo Suzuki† and Yuichi Tanaka‡
*The University of Kitakyushu, Japan, Email: s-kyochi@kitakyu-u.ac.jp
† University of Tsukuba, Japan, Email: taizo@cs.tsukuba.ac.jp
‡ Tokyo University of Agriculture and Technology, Japan, Email: ytnk@cc.tuat.ac.jp

***Abstract*—This paper aims to design a new two-dimensional (2D) non-separable implementation of dyadic-valued cosine-sine modulated filter banks (2D D-CSMFBs) for low computational complexity. CSMFBs satisfy rich directional selectivity (DS) and shift-invariance (SI), and they can be easily designed by the modulation of a prototype filter. In addition, our previous work introduced a one-dimensional (1D) D-CSMFBs (1D D-CSMFBs). By restricting real-valued filter coefficients to rational-valued ones, they can save computational cost while keeping DS and SI. The proposed 2D implementation in this paper can further reduce the computational cost by unifying the conventional 2D separable structure into a 2D non-separable one directly. Furthermore, experimental results of image non-linear approximation show that the proposed 2D D-CSMFBs are comparable or even better than the 1D D-CSMFBs.**

I. Introduction

For decades, various extensions of discrete wavelet transform, which satisfy "rich directional selectivity[1]" (DS), have been widely studied and presented, such as *Contourlet* [1], *Curvelet* [2], *Shearlet* [3], and so on. Among them, dual-tree complex wavelet transforms (DTCWTs) have been paid much attention due to their low redundancy and low computational complexity [4]. While directional selectivity usually increases redundancy or computational complexity, DTCWTs can restrict their redundancy ratio to 2 and save computational complexity by two-dimensional (2D) separable implementation of parallel DWTs, i.e., cascading the filtering along vertical and horizontal directions. Furthermore, it also satisfies "shift-invariance[2]" (SI). Thanks to DS and SI, it can be successfully applied to various kinds of practical image processing, such as image denoising, image analysis, image compression.

As well as the DTCWT, another DS and SI transforms, cosine-sine modulated filter banks (CSMFBs), have been shown recently [5]. DTCWT is difficult to design M-channel cases with good filter performances, e.g., stopband attenuation or coding gain, due to the fractional delay requirement imposed on parallel DWTs, which degrades design degree of freedom. On the other hand, because CSMFBs require NO fractional delay requirement (just the modulation of prototype filter), M-channel CSMFBs can be better performance than M-channel DTCWTs and effectively work in application.

In this paper, we address on finding a simplified structure of CSMFBs for low computational complexity. In [6], one-dimensional dyadic-valued CSMFBs (1D D-CSMFBs) based on lifting structure have been introduced. Despite of real-rational conversion, 1D D-CSMFBs can still keep DS and SI properties and show better performance compared with 1D rational-valued DTCWTs (D-DTCWT) [7]. However, since the previous structure does NOT consider removing redundant lifting steps, there is possibility to exist much simpler structure of 1D D-CSMFBs.

This paper presents a new 2D non-separable implementation of D-CSMFBs (2D D-CSMFBs) for lower computational complexity. While the conventional 2D transform of 1D D-CSMFBs is based on separable implementation, the proposed implementation consists of a 2D non-separable structure via Kronecker product. Due to this 2D unification, redundant lifting steps can be removed and lower computational complexity can be achieved. Moreover, in spite of the simplification, experimental results of image non-linear approximation (NLA) show that 2D D-CSMFBs has the comparable or even better performance than 2D separable structure.

Notations: $j := \sqrt{-1}$. $H(z)$ is defined as $H(z) := \sum_n h(n)z^{-n}$. The (M, L) FB means the M-channel filter bank with the filter length of L. The $(M \times M, L \times L)$ 2D FB means the $M \times M$-channel filter bank with the filter size of $L \times L$. $\mathbf{I}$, $\mathbf{J}$, and $\mathrm{diag}(a_0, \ldots, a_{N-1})$ are the identity, the reversal identity, and the diagonal matrices, respectively. $\mathbf{\Gamma} = \mathrm{diag}(1, -1, \ldots, 1, -1)$.

II. Review

A. Dual-Tree Complex Wavelet Transform

DTCWTs are constructed by two maximally decimated perfect reconstruction (PR) FBs, as illustrated in Fig. 1. In this case, the pair $\{H_k^{(1)}(z), H_k^{(2)}(z)\}$ $(0 \le k \le M-1)$ is designed to satisfy the following equations [4]:

$$H_k^{(2)}(e^{j\omega}) = e^{-j\theta_k(\omega)} H_k^{(1)}(e^{j\omega}), \tag{1}$$
$$\theta_0(\omega) = \left(d + \frac{1}{2}\right)(M-1)\omega - p\omega,$$

[1]Directional selectivity means sparse representation capability for directionally oriented components of images, e.g., lines and edges. For that, basis functions should be oriented along various kinds of directions [4].

[2]Shift-invariance means the stability of wavelet coefficients under the shift of input signals [4].

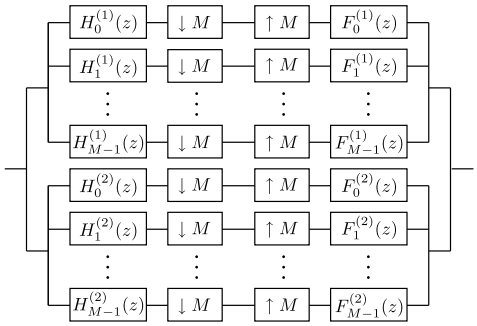

Fig. 1. M-channel DTCWTs and CSMFBs

where $d \in \mathbb{Z}$ denotes the delay between the primal FB and the dual FB, $\forall p \in \left\{0, \ldots, \left\lceil \frac{M}{2} \right\rceil - 1\right\}, \forall \omega \in \left[\frac{2\pi}{M}p, \frac{2\pi}{M}(p+1)\right)$, and

$$\theta_k(\omega) = \begin{cases} \frac{\pi}{2} - \left(d + \frac{1}{2}\right)\omega & \omega \in (0, 2\pi) \\ 0 & \omega = 0, \end{cases} \tag{2}$$

where $1 \le k \le M-1$. Practically, M-channel DTCWTs are designed by the dual-tree complex wavelet packet (DTCWP) [8] which cascades 2-channel DTCWTs and 2-channel PRFBs.

B. Cosine-Sine Modulated Filter Banks

As well as DTCWTs, a CSMFB also consists of two maximally decimated filter banks as in Fig. 1. Its filter coefficients of $\{H_k^{(1)}(z), H_k^{(2)}(z)\}$ are expressed as [5]:

$$\begin{cases} h_k^{(1)}(n) := 2p(n)\cos\left((k+\frac{1}{2})\frac{\pi}{M}\left(n - \frac{N-1}{2}\right) + \theta_k\right) \\ h_k^{(2)}(n) := 2p(n)\sin\left((k+\frac{1}{2})\frac{\pi}{M}\left(n - \frac{N-1}{2}\right) + \theta_k\right) \end{cases} \tag{3}$$

where $k = 0, \ldots, M-1$, $\theta_k = (-1)^k \frac{\pi}{4}$ and $p(n)$ is the prototype filter. In the paraunitary CSMFB, $h_k^{(2)}(n) = (-1)^k f_k^{(1)}(n) = (-1)^k h_k^{(1)}(N-1-n)$. Thus, if the primal FB satisfies the PR property, the dual FB system also satisfies it. Our previous work clarified the relationship of cosine and sine modulation derived both DS and SI [5].

The polyphase matrices $\mathbf{E}^{(1)}(z)$ and $\mathbf{E}^{(2)}(z)$ corresponding to the CMFB and the SMFB can be decomposed as lattice structures. They can be expressed by [9]:

$$\begin{aligned} \mathbf{E}^{(1)}(z) =& \mathbf{C}_{\mathrm{IV}}\mathbf{W}\mathbf{\Lambda}(z)\mathbf{D}_0^{(1)}\prod_{k=1}^{K-1}\left(\mathbf{\Lambda}(z^2)\mathbf{D}_k^{(1)}\right) \\ \mathbf{D}_k^{(1)} =& \begin{bmatrix} -\mathbf{C}_k & \mathbf{S}_k\mathbf{J} \\ \mathbf{J}\mathbf{S}_k & \mathbf{J}\mathbf{C}_k\mathbf{J} \end{bmatrix}, \mathbf{\Lambda}(z) = \begin{bmatrix} z^{-1}\mathbf{I} & \mathbf{0} \\ \mathbf{0} & \mathbf{I} \end{bmatrix}, \end{aligned} \tag{4}$$

$$\begin{aligned} \mathbf{E}^{(2)}(z) =& \mathbf{S}_{\mathrm{IV}}\mathbf{W}\mathbf{\Lambda}(z)\mathbf{D}_0^{(2)}\prod_{k=1}^{K-1}\left(\mathbf{\Lambda}(z^2)\mathbf{D}_k^{(2)}\right) \\ \mathbf{D}_k^{(2)} =& \begin{bmatrix} \mathbf{C}_k & \mathbf{S}_k\mathbf{J} \\ \mathbf{J}\mathbf{S}_k & -\mathbf{J}\mathbf{C}_k\mathbf{J} \end{bmatrix} = \begin{bmatrix} \mathbf{I} & \mathbf{0} \\ \mathbf{0} & -\mathbf{I} \end{bmatrix}\mathbf{D}_k^{(1)}\begin{bmatrix} -\mathbf{I} & \mathbf{0} \\ \mathbf{0} & \mathbf{I} \end{bmatrix}. \end{aligned} \tag{5}$$

where $\mathbf{C}_k = \mathrm{diag}\left(\cos\theta_{k0}, \ldots, \cos\theta_{k\ M/2-1}\right)$, $\mathbf{S}_k = \mathrm{diag}\left(\sin\theta_{k0}, \ldots, \sin\theta_{k\ M/2-1}\right)$, $\mathbf{W} = \begin{bmatrix} \mathbf{0} & \mathbf{I} \\ \mathbf{I} & \mathbf{0} \end{bmatrix}$, and $\mathbf{C}_{\mathrm{IV}}$ and $\mathbf{S}_{\mathrm{IV}}$ denote the type-IV DCT and DST, respectively. The structure is depicted in Fig. 2 (a).

C. Dyadic-Valued Implementation of CSMFB and DTCWT

In general, the rotation matrix can be factorized into lifting steps as follows [10]:

$$\begin{bmatrix} \cos\theta & -\sin\theta \\ \sin\theta & \cos\theta \end{bmatrix} = \begin{bmatrix} 1 & p \\ 0 & 1 \end{bmatrix}\begin{bmatrix} 1 & 0 \\ u & 1 \end{bmatrix}\begin{bmatrix} 1 & p \\ 0 & 1 \end{bmatrix}, \tag{6}$$

where $p = \frac{\cos\theta - 1}{\sin\theta}$, $u = \sin\theta$ are called lifting coefficients. The lifting factorization enables us to design rational-valued transformation simply by rounding lifting coefficients $r_p = \mathrm{round}(p \times 2^N)/2^N$, $r_u = \mathrm{round}(u \times 2^N)/2^N$, while preserving PR condition. By converting each rational-valued multiplication with rounding operation to additions and bit-shifters, for example,

$$r_p = \frac{P}{2^N} = \alpha_\ell 2^\ell + \alpha_{\ell-1}2^{\ell-1} + \cdots, \tag{7}$$

where P, $\ell \in \mathbb{Z}$, and $\alpha_k = 1$ or 0 $(k \le \ell)$, a multiplierless CSMFB can be achieved. As shown in Fig. 2 (b), each $\mathbf{D}_k^{(1)}$ can be reduced as

$$\mathbf{D}_k^{(1)} = \begin{bmatrix} -\mathbf{I} & \mathbf{0} \\ \mathbf{0} & \mathbf{I} \end{bmatrix}\begin{bmatrix} \mathbf{I} & \mathbf{P}_k\mathbf{J} \\ \mathbf{0} & \mathbf{I} \end{bmatrix}\begin{bmatrix} \mathbf{I} & \mathbf{0} \\ \mathbf{J}\mathbf{U}_k & \mathbf{I} \end{bmatrix}\begin{bmatrix} \mathbf{I} & \mathbf{P}_k\mathbf{J} \\ \mathbf{0} & \mathbf{I} \end{bmatrix}, \tag{8}$$

where $\mathbf{P}_k = \mathrm{diag}\left(p_{k0}, \ldots, p_{kM/2-1}\right)$ and $\mathbf{U}_k = \mathrm{diag}\left(u_{k0}, \ldots, u_{kM/2-1}\right)$. Since $\mathbf{C}_{\mathrm{IV}}$ is constructed by some rotation and butterfly matrices [11], it can also be converted to a lifting-based factorization. Similarly, according to the relationship of $\mathbf{D}_k^{(1)}$ and $\mathbf{D}_k^{(2)}$, and $\mathbf{S}_{\mathrm{IV}} = \Gamma\mathbf{C}_{\mathrm{IV}}\mathbf{J}$, both $\mathbf{D}_k^{(2)}$ and $\mathbf{S}_{\mathrm{IV}}$ can be expressed by a lifting factorization. Interestingly, the lifting coefficients for $\mathbf{E}^{(1)}(z)$ can be reused for $\mathbf{E}^{(2)}(z)$.

On the other hand, M-channel D-DTCWT is designed based on the lifting factorization of all 2-channel DTCWTs and 2-channel FBs used in wavelet packets [7].

III. Two-dimensional Rational-valued Cosine-Sine Modulated Filter Banks Based on the Lifting Factorization

A. The Proposed Structure

This section derives a non-separable structure of 2D D-CSMFB from separable 2D implementation. In general, a 1D FB is applied to images in separable way. Specifically, each building block, e.g., $\mathbf{D}_k^{(1)}$ in a lattice structure (4), is applied to a local block $\mathbf{X}$ in a image as:

$$\mathbf{Y} = \mathbf{D}_k^{(1)}\mathbf{X}(\mathbf{D}_k^{(1)})^T, \tag{9}$$

where $\mathbf{Y}$ is the output block. The separable (lifting) implementation for (9) is illustrated in Fig. 3.

Here, by letting $\mathbf{x}$ be the 1D vector by rearranging the 2D block $\mathbf{X}$, the operation (9) can be reformulated as

$$\mathbf{y} = \mathbf{D}_k^{(1)} \otimes \mathbf{D}_k^{(1)}\mathbf{x}, \tag{10}$$

where $\otimes$ denotes Kronecker product. Since multiplication of $\mathbf{D}_k^{(1)}$ is essentially based on 2×2 matrices as shown in Fig.

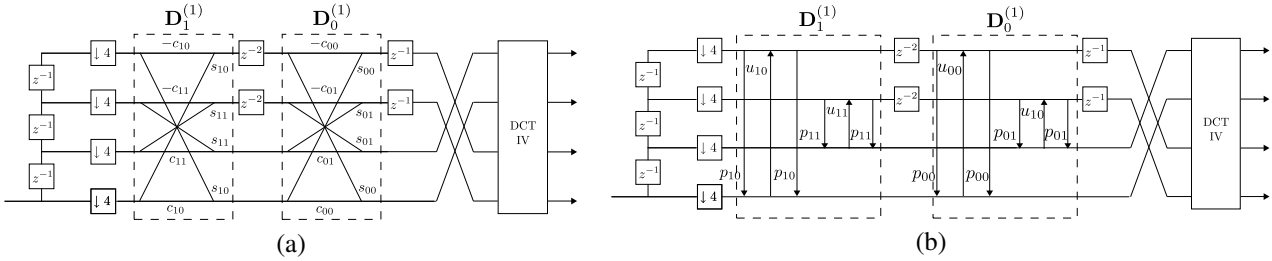

Fig. 2. The structure of the 4 channel CMFBs. (a) rotation-matrix-based structure, (b) lifting-based structure

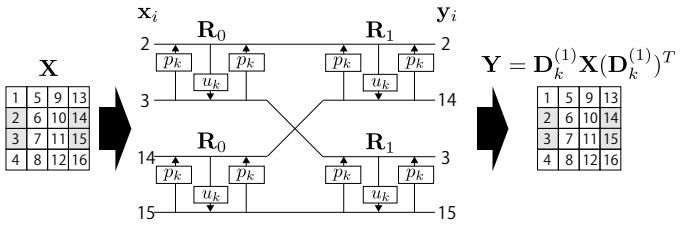

Fig. 3. An example of the separable lifting implementation for (11).

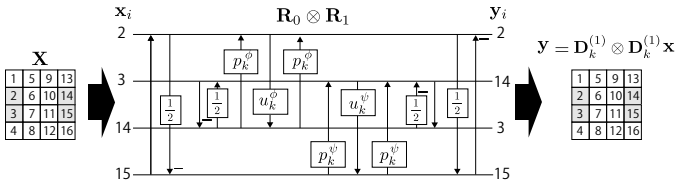

Fig. 4. An example of the direct 2D lifting implementation for (12). p_k^{ϕ}, u_k^{ϕ}, p_k^{ψ}, and u_k^{ψ} denote the lifting coefficients obtained from $\mathbf{\Phi}_{m,m}$ and $\mathbf{\Psi}_{m,m}$.

2(a), (10) can be reduced to several submatrix multiplications expressed as follows:

$$\begin{aligned}\mathbf{y}_i &= \begin{bmatrix}\mathbf{R}_m^{(k)} & \\ & \mathbf{R}_m^{(k)}\end{bmatrix}\mathbf{P}_0\begin{bmatrix}\mathbf{R}_n^{(k)} & \\ & \mathbf{R}_n^{(k)}\end{bmatrix}\mathbf{x}_i \qquad (11)\\ &= \mathbf{R}_m^{(k)} \otimes \mathbf{R}_n^{(k)}\mathbf{x}_i \quad (0 \le m, n \le M/2-1),\\ \mathbf{R}_m^{(k)} &= \begin{bmatrix}R_{00}^{(k,m)} & R_{01}^{(k,m)}\\ R_{10}^{(k,m)} & R_{11}^{(k,m)}\end{bmatrix} = \begin{bmatrix}-\cos\theta_{km} & \sin\theta_{km}\\ \sin\theta_{km} & \cos\theta_{km}\end{bmatrix},\end{aligned}$$

where $\mathbf{P}_0$ denotes the permutation matrix corresponding to Fig. 3 and $\mathbf{x}_i$ $(0 \le i \le M/2-1)$ is the part of $\mathbf{x}$. For example in Fig. 3, $\mathbf{x}_i = [X_2, X_3, X_{14}, X_{15}]^T$, where X_k denotes the sample at the index of k in $\mathbf{X}$. The Kronecker product of $\mathbf{R}_m^{(k)} \otimes \mathbf{R}_n^{(k)}$ can be factorized as the following equation:

$$\begin{aligned}&\mathbf{R}_m^{(k)} \otimes \mathbf{R}_n^{(k)} = \mathbf{H}\mathbf{\Gamma}_0\mathbf{R}_{m,n}^{(k)}\mathbf{\Gamma}_1\mathbf{H} \qquad (12)\\ &\mathbf{R}_{m,n}^{(k)} = \begin{bmatrix}\cos\phi_{m,n} & 0 & \sin\phi_{m,n} & 0\\ 0 & \cos\psi_{m,n} & 0 & \sin\psi_{m,n}\\ \sin\phi_{m,n} & 0 & -\cos\phi_{m,n} & 0\\ 0 & \sin\psi_{m,n} & 0 & -\cos\psi_{m,n}\end{bmatrix},\\ &\phi_{m,n} = \theta_m - \theta_n, \quad \psi_{m,n} = \theta_m + \theta_n,\\ &\mathbf{\Gamma}_0 = \mathrm{diag}(1,-1,-1,1), \quad \mathbf{\Gamma}_1 = \mathrm{diag}(1,1,-1,-1),\\ &\mathbf{H} = \frac{1}{\sqrt{2}}\begin{bmatrix}1 & 0 & 0 & 1\\ 0 & 1 & 1 & 0\\ 0 & 1 & -1 & 0\\ 1 & 0 & 0 & -1\end{bmatrix}.\end{aligned}$$

This factorization is analogous to the one for hierarchical lapped biorthogonal transform (HLBT) employed in JPEG XR [12]. Since $\mathbf{\Phi}_{m,n} := \begin{bmatrix}\cos\phi_{m,n} & \sin\phi_{m,n}\\ \sin\phi_{m,n} & -\cos\phi_{m,n}\end{bmatrix}$ and $\mathbf{\Psi}_{m,n} := \begin{bmatrix}\cos\psi_{m,n} & \sin\psi_{m,n}\\ \sin\psi_{m,n} & -\cos\psi_{m,n}\end{bmatrix}$ can be factorized into 3 lifting steps as in (6). Moreover, by moving some scaling factors $\mathrm{diag}(\sqrt{2}, \frac{1}{\sqrt{2}}, \sqrt{2}, \frac{1}{\sqrt{2}})$ of the right $\mathbf{H}$ to the left $\mathbf{H}$ in (12) or vice versa, both $\mathbf{H}$ can be further decomposed into lifting steps as shown in Fig. 4. Note that when indices m and n are same, $\mathbf{\Phi}_{m,m}$ becomes $\begin{bmatrix}1 & 0\\ 0 & -1\end{bmatrix}$, the number of multiplications can be reduced.

In the proposed method, a different lifting factorization of type-IV DCT is used compared with [11], which is expressed as follows [14]:

$$\begin{aligned}&\mathbf{C}_{\mathrm{IV}} = \mathbf{S}\mathbf{P}_1\begin{bmatrix}\mathbf{C}_{\mathrm{II}} & \mathbf{0}\\ \mathbf{0} & \mathbf{C}_{\mathrm{II}}\mathbf{\Gamma}\end{bmatrix}\mathbf{T}, \mathbf{T} = \begin{bmatrix}\mathbf{T}_{\cos} & \mathbf{T}_{\sin}\mathbf{J}\\ \mathbf{J}\mathbf{T}_{\sin} & -\mathbf{J}\mathbf{T}_{\cos}\mathbf{J}\end{bmatrix},\\ &\left[\mathbf{T}_{\cos}\right]_{kk} = \cos\left(\frac{(2k+1)\pi}{4M}\right), \left[\mathbf{T}_{\sin}\right]_{kk} = \sin\left(\frac{(2k+1)\pi}{4M}\right),\\ &\mathbf{S} = \begin{bmatrix}1 & & & & \\ & \mathbf{R}_{\pi/4} & & & \\ & & \ddots & & \\ & & & \mathbf{R}_{\pi/4} & \\ & & & & 1\end{bmatrix}, \mathbf{R}_{\pi/4} = \frac{1}{\sqrt{2}}\begin{bmatrix}1 & 1\\ -1 & 1\end{bmatrix},\end{aligned}$$

$\mathbf{C}_{\mathrm{II}}$ is the type-II DCT and $\mathbf{P}_1$ is a permutation matrix, respectively. $\mathbf{S}$ and $\mathbf{T}$ can be decomposed into 2D lifting steps with the same way.

The 2D lifting implementation of the SMFB $\mathbf{E}^{(2)}(z)$ can be realized in the same way of the CMFB.

B. Computational Complexity

This section discusses about computational complexity of 1D and 2D D-CSMFBs in terms of the number of lifting steps per block. As shown in Fig. 3, in order to process an $M \times M$ block, the separable implementation requires $3 \times 4 \times \left(\frac{M}{2}\right)^2 = 3M^2$ lifting steps. On the other hand, a direct 2D implementation consists of $6 \times \left(\frac{M}{2}\right)^2 - 3 \times M/2 = \frac{3}{2}(M^2 - M)$ lifting steps. The total number of additions and

TABLE I
THE NUMBER OF ADDITIONS AND BIT-SHIFTERS

Separable D-DTCWT (8×8-channel, 22×22-tap)					
Word length	8 bit	7 bit	6 bit	5 bit	4 bit
additions	2464	2224	2096	1232	1232
bit-shifters	2464	2224	2096	1232	1232
Separable 1D D-CSMFB (8×8-channel, 16×16-tap)					
Word length	8 bit	7 bit	6 bit	5 bit	4 bit
additions	2352	2096	1920	1584	1360
bit-shifters	2288	2032	1856	1520	1296
Non-separable 2D D-CSMFB (8×8-channel, 16×16-tap)					
Word length	8 bit	7 bit	6 bit	5 bit	4 bit
additions	1477	1332	1242	1017	930
bit-shifters	1461	1316	1226	1001	913

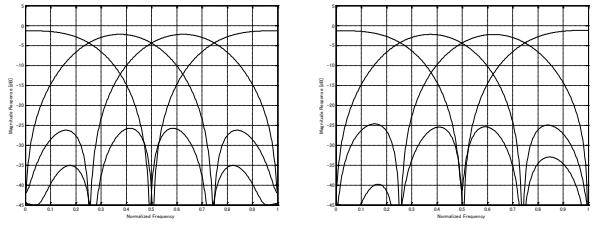

(a) Real (b) Rational

Fig. 5. Frequency responses of the designed $(4, 8)$ CSMFB. (a): Real-valued CSMFB, (b) Rational-valued CSMFB with 5 bit lifting coefficients.

bit-shifters of a designed CSMFB depends on the number of additions and bit-shifters allocated to each lifting coefficients.

IV. SIMULATION

In this section, practical computational complexity and NLA performance of 2D D-CSMFBs are shown. In order to construct 2D D-CSMFBs and 1D D-CSMFBs, M-channel CSMFBs are firstly designed. As a comparison, M-channel DTCWT is designed by using DTCWP [8] cascading a 2-channel DTCWT [4] and 2-channel PUFBs. Both transforms are optimized to minimize the stopband attenuation Δ specified by

$$\Delta = \sum_{k=0}^{M-1} \int_{\Omega_s(k)} |H_k^{(1)}(e^{j\omega})|^2 d\omega, \tag{13}$$

where $\Omega_s(k)$ is stoppband of the $H_k^{(1)}(e^{j\omega})$, $(0 \le k \le M-1)$. In this paper, we set as $\Omega_s(k) = [0, \frac{\pi}{M}(k-2)] \cup [\frac{\pi}{M}(k+2), \pi]$. If $\frac{\pi}{M}(k-2) \le 0$ or $\frac{\pi}{M}(k+2) \ge \pi$, the corresponding interval is ignored. Then, each optimized transform is decomposed via lifting factorization and performed rounding for constructing 1D and 2D D-CSMFBs and D-DTCWT. Fig. 5 depicts the frequency responses of the designed $(4, 8)$ CSMFB and D-CSMFB (# of channel, # of filter length). Note that, our previous work [6] shows that the results of stopband attenuation of 1D CSMFBs are consistently superior to those of DTCWTs. It is because the design degree of freedom of DTCWTs is quite limited, due to the packet implementation. For example, the number of the filter length of the cascaded 2-channel PUFBs for the $(4, 16)$ and $(8, 22)$ D-DTCWTs is 4.

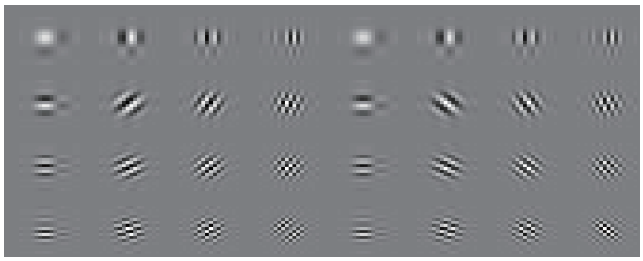

Fig. 6. 32 directional basis functions with size of 16×16 obtained by the 2D CSMFB whose lifting coefficents are rounded to 4 bit word length.

Based on the designed lifting coefficients of CSMFBs, the 2D D-CSMFBs are constructed. Table I clearly shows that the 2D D-CSMFBs require fewer addition and bit-shifters than the D-DTCWT and the 1D D-CSMFB. In addition, the 2-D wavelet basis functions obtained by the 4×4-channel 2D D-CSMFB are shown in Fig. 6. Clearly, the basis functions are oriented under rounding operation.

A. Non-Linear Approximation

Non-linear approximation (NLA) [13] is often used as a criteria of transform effectiveness for practical applications, e.g., image coding, denoising, and so on. In this section, NLA is demonstrated in the following way. Let f, $c_{1,n}$ and $c_{2,n}$ be the input image and the transformed coefficients of the primal FB and the dual FB, e.g., the CMFB and the SMFB. In addition, f_M is defined as the reconstructed signal obtained from the M-largest coefficients within $\{c_{1,n}\}, \{c_{2,n}\}$ by performing the inverse transform. The accuracy of NLA $\|f - f_M\|$ indicates how well the transform compacts the energy of the input signal.

Here we evaluated the $(8, 22)$ D-DTCWT, the $(8, 16)$ 1D D-CSMFB, and the $(8 \times 8, 16 \times 16)$ 2D D-CSMFB using typical test images *Lena* and *Barbara* (512×512 pixels). For all the transforms, the number of 2D decomposition level is set to 2. Periodical extension is used for image boundary processing. For reconstruction, 3% transformed coefficients of *Lena* and 6% transformed coefficients of *Barbara* are kept.

Table II shows the NLA PSNR results versus the number of bit word length allocated to lifting coefficients in each transform. Although the 1D D-CSMFB shows higher PSNRs in the case of high bit word length, it suffers from degradation of performance in low bit word length, and the proposed 2D D-CSMFB can achieve comparable or even better performance compared with D-DTCWT and 1D D-CSMFB in low bit word length. Fig. 7 shows the 2D D-CSMFB provides the best visual quality even the case of lowest bit word length (5 bit). Since the 2D D-CSMFB has less lifting steps (rounding produces filter perfromance degradation), it is more stable in low bit word length than the 1D D-CSMFB.

V. CONCLUSION

In this paper we proposed the 2D implementation of D-CSMFBs for low computational complexity. By unifying the conventional 1D D-CSMFB via Kronecker product, redundant

TABLE II
NON-LINEAR APPROXIMATION

Lena (3% coeffs): D-DTCWT (8×8-channel, 22×22-tap)					
Word length	5 bit	6 bit	7 bit	8 bit	32 bit
PSNR [dB]	29.200	29.361	29.367	29.384	29.381
Lena (3% coeffs): 1D D-CSMFB (8×8-channel, 16×16-tap)					
Word length	5 bit	6 bit	7 bit	8 bit	32 bit
PSNR [dB]	27.668	28.064	30.912	31.023	31.035
Lena (3% coeffs): 2D D-CSMFB (8×8-channel, 16×16-tap)					
Word length	5 bit	6 bit	7 bit	8 bit	32 bit
PSNR [dB]	**30.168**	**30.335**	**30.363**	**30.472**	**30.599**
Barbara (6% coeffs): D-DTCWT (8×8-channel, 22×22-tap)					
Word length	5 bit	6 bit	7 bit	8 bit	32 bit
PSNR [dB]	28.972	29.084	29.0931	29.103	29.113
Barbara (6% coeffs): 1D D-CSMFB (8×8-channel, 16×16-tap)					
Word length	5 bit	6 bit	7 bit	8 bit	32 bit
PSNR [dB]	28.502	28.697	31.471	31.542	31.543
Barbara (6% coeffs): 2D D-CSMFB (8×8-channel, 16×16-tap)					
Word length	5 bit	6 bit	7 bit	8 bit	32 bit
PSNR [dB]	**30.825**	**30.963**	**30.975**	**31.050**	**31.142**

lifting steps can be removed from the entire transform. The design examples in simulation require much fewer number of additions and bit-shifters than the D-DTCWT and the 1D D-CSMFB. Even if the 2D unification and rounding lifting coefficients is introduced, simulation results show 2D D-CSMFB keep good directional selectivity. Finally, in the NLA simulation, it is clarified that the 2D D-CSMFB is robust for low bit word length allocation, and thus provides better numerical and visual reconstruction quality compared with D-DTCWT and 1D D-CSMFB.

ACKNOWLEDGMENT

This work was supported by JSPS KAKENHI Grant Number 24860055, 25820152.

REFERENCES

[1] M. N. Do and M. Vetterli, "The contourlet transform: An efficient directional multiresolution image representation," *IEEE Trans. Image Process.*, vol. 14, no. 12, pp. 2091–2106, Dec. 2005.

[2] E. J. Candès and D. L. Donoho, "New tight frames of curvelets and optimal representations of objects with piecewise C^2 singularities," Comm. Pure Appl. Math., vol. 56, no. 2, pp. 219–266, Feb. 2004.

[3] S. Yi, D. Labate, G. R. Easley, and H. Krim, "A shearlet approach to edge analysis and detection," *IEEE Trans. Image Process.*, vol. 18, no. 5, pp. 929–941, May 2009.

[4] I. W. Selesnick, R. G. Baraniuk and N. C. Kingsbury, "The dual-tree complex wavelet transform," *IEEE Signal Process. Magazine*, vol. 22 pp. 123–151, Nov. 2005.

[5] S. Kyochi, T. Uto, M. Ikehara, "Dual-tree complex wavelet transform arising from cosine-sine modulated filter banks," in *Proc. ISCAS*, Taipei, Taiwan, pp.2189-2192, May 2009.

[6] S. Kyochi, T. Suzuki, Y. Tanaka, "A directional and shift-invariant transform based on M-channel rational-valued cosine-sine modulated filter banks," in *Proc. APSIPA ASC*, Hollywood, CA, Dec. 2012.

[7] A. Abbas and Trac D. Tran, "Rational coefficient dual-tree complex wavelet transform: design and implementation," *IEEE Trans. Signal Process.*, vol. 56, no. 8, pp. 3523–3534, Aug. 2008.

[8] I. Bayram and I. W. Selesnick, "On the dual-tree complex wavelet packet and M-band transform," *IEEE Trans. Signal Process.*, vol. 56, no. 6, pp. 2298–2310, June 2008.

[9] A. Viholainen, J. Alhava and M. Renfors, "Implementation of parallel cosine and sine modulated filter banks for equalized transmultiplexer systems," in *Proc. ICASSP*, vol. 6, pp. 3625–3628, Salt Lake City, UT, June 2001.

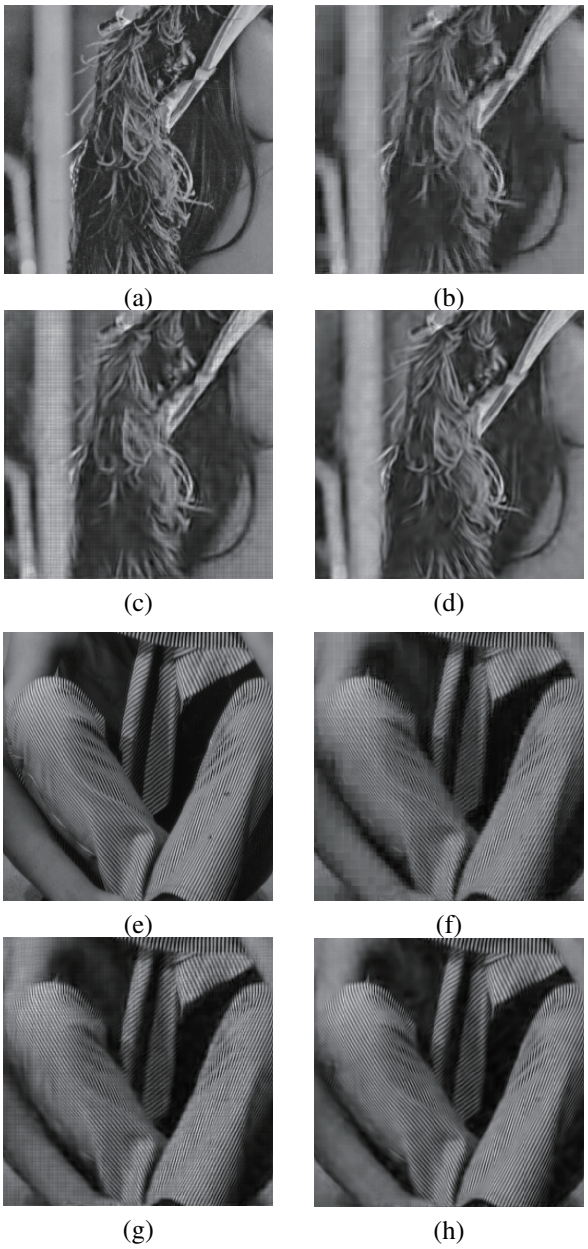

Fig. 7. NLA results. (a) and (e): Original images of (zoomed) *Lena* and *Barbara* (b) and (f): D-DTCWT (8×22, Bit word length: 5 bit) (c) and (g): 1D D-CSMFB (8×16, Bit word length: 5 bit) (d) and (h): 2D D-CSMFB (8×16, Bit word length: 5 bit).

[10] I. Daubechies and W. Sweldens, "Factoring wavelet transforms into lifting steps," *J. Fourier Anal. Appl.*, vol. 4, no. 3, pp. 245-267, 1998.

[11] Z. Wang, "Fast algorithms for the discrete W transform and for the discrete fourier transform," *IEEE Trans. Signal Process.*, vol. 40, no. 11, pp. 803–816, June 1984.

[12] C. Tu, S. Srinivasan, G. J. Sullivan, S. Regunathan, and H. S. Malvar, "Low-complexity hierarchical lapped transform for lossy-to-lossless image coding in JPEG XR / HD Photo," in *Proc. of SPIE Applications of Digital Image Processing XXXI*, San Diego, CA, August 2008.

[13] S. Mallat, *A Wavelet Tour of Signal Processing: The Sparse Way,* 3rd ed. New York: Academic, 2008.

[14] Z. Wang, "On computing the discrete fourier and cosine transforms," *IEEE Trans. Acoust. Speech Signal Process.*, Vol. 33, No. 4, pp. 1341-1344, 1985.

[15] S. Malvar, "Extended lapped transforms: properties, applications and fast algorithms," *IEEE Trans. Signal Process.*, vol. 40, no. 11, pp. 2703–

2714, June 1992.